Analyst

PAPER

Cite this: *Analyst*, 2014, **139**, 2379

Selective visual detection of trace trinitrotoluene residues based on dual-color fluorescence of graphene oxide–nanocrystals hybrid probe†

Kui Zhang,‡[a] Lei Yang,‡[b] Houjuan Zhu,[a] Fang Ma,[a] Zhongping Zhang[a] and Suhua Wang*[a]

Received 26th December 2013
Accepted 12th February 2014

DOI: 10.1039/c3an02380j

www.rsc.org/analyst

Herein, for the detection of highly explosive 2,4,6-trinitrotoluene (TNT) instantly and on-site, a fluorescence ratiometric probe using a dual-emission nanohybrid has been developed. The nanohybrid comprises blue-colored fluorescent graphene oxide (FGO) being conjugated with red-emitting manganese-doped ZnS nanocrystals (ZnS:Mn NCs), the latter being functionalized with hexamethylenediamine. The blue fluorescence of FGO is insensitive to TNT and is used as an internal reference, whereas the red fluorescence of ZnS:Mn NCs can be selectively quenched by TNT through electron transfer, resulting in a unique red–purple–blue color response as the amount of TNT is increased. Thus, the probe could be used for the quantitative measurement of TNT based on the fluorescence ratiometric method. We demonstrated that the nanohybrid probe exhibited high visual detection sensitivity and reliability in comparison with single-color fluorescence quenching probes. A fluorescence test paper was prepared using the nanohybrid probe and was demonstrated to detect TNT residues directly on various surfaces including rubber, a person's fingers and manila envelopes with a visual detection limit as low as 5.68 ng mm^{-2}, showing its promising application for security screening.

Introduction

The detection of illegally transported explosives has become more important since the rising threat of global terrorism.[1–7] 2,4,6-Trinitrotoluene (TNT) is a potent explosive for terror attacks, so its detection on suspicious objects is important for the safety of airports, mail sorting centers and other civilian situations. Various methods involving in complex instrumentation such as chromatography–mass spectrometry,[8–11] ion mobility spectrometry,[12,13] Raman spectroscopy,[14–16] terahertz spectroscopy,[17,18] and X-ray dispersion,[19,20] have been developed for the detection of TNT. These instrumental techniques are highly selective and sensitive, but most of these devices are rather bulky, expensive, and time-consuming, and the detection process is usually to be analyzed in laboratory. Therefore, instant detection and on-site identification of trace TNT residues on the surface of suspicious objects is still challenging and in great demand. We previously reported a ratiometric fluorescence probe for the visual detection of TNT, which was prepared through a complicated procedure of hybridizing two different-sized CdTe quantum dots.[31] Herein, we report a novel probe for TNT detection which was synthesized through a simplified procedure and used less toxic material, graphene and manganese-doped ZnS nanocrystals. The fluorescent red-colored nanocrystal as the recognition unit specific for TNT and fluorescent blue-colored graphene oxide as a stable internal reference. This probe generates ratiometric fluorescence as a signal output for the visual indication of TNT presence.

Fluorescence sensing of TNT has been developed widely based on fluorescent conjugated polymers, polymer films, nanoparticles, and other chemosensors.[21–37] Most of these chemosensors contain fluorescent organic dyes, which are usually susceptible to photobleaching, low fluorescence quantum yield and low signal intensities. In addition, many researchers have also focused on fluorescence nanosensors employing luminescent nanomaterials as the signal output such as quantum dots,[30–33] metal nanoclusters,[34] dye-doped nanoparticles,[35–37] and so on, in which the sensing method is highly attractive because their sensitivity and selectivity are significantly improved by chemical modification on the surface of nano-sized materials. Most of these sensors based on single-color fluorescence intensity changes tend to suffer interference from a variety of factors, such as the probe molecule concentration, excitation intensity, instrumental efficiency, and environmental conditions, and also do not provide good opportunities for

[a]*Institute of Intelligent Machines, Chinese Academy of Sciences, Hefei, Anhui 230031, China. E-mail: shwang@iim.ac.cn*

[b]*Department of Chemical Physics, University of Science and Technology of China, Hefei, Anhui 230026, China*

† Electronic supplementary information (ESI) available: Infrared transmission spectroscopy, TEM images, the stability of the nanohybrid probe, absorption and fluorescence spectra. See DOI: 10.1039/c3an02380j

‡ These two authors contributed equally to this work.

visualization of the detection. By contrast, methods based on dual-color fluorescence for ratiometric measurement are less prone to suffering such problems due to their self-calibration of two emission bands.[38–43] Furthermore, these sensing methods not only allow more precise measurement and quantitative analysis by changing in the ratio of the fluorescence intensities at two wavelengths, but can also achieve visual identification by observing color changes when the analyte leads to a change of the two emissions with different colors of a ratiometric sensor. Therefore, although the fluorescence-based protocol has been widely used for TNT sensing, the development of a novel dual-color fluorescence sensor based on a ratiometric signal output for the naked eye detection of TNT is of particular interest because of its practical demand for public security.

We design a novel fluorescence probe comprising manganese-doped ZnS nanocrystals (ZnS:Mn NCs) and fluorescent graphene oxide (FGO) with dual-emission bands and establish its utility for the rapid and visual identification of TNT. As illustrated in Scheme 1, the dual-color fluorescence nanohybrid probe has two peaks under a single wavelength excitation, in which the blue-colored fluorescence of FGO is insensitive to TNT and the red-colored fluorescence of the NCs is specifically sensitive to TNT. The ratiometric fluorescence responses are therefore realized upon quenching of the red fluorescence of NCs by TNT while the blue-colored fluorescence intensity of FGO is relatively stable. A small variation of the ratio of the two intensities leads to distinct change in the fluorescence color of the probe, which can be easily observed by the naked eye under a UV lamp. We further demonstrate the utility of the nanohybrid probe for the visual detection of TNT residues on various surfaces including rubber, a person's fingers and manila envelopes through the fluorescence color changes. This method shows high selectivity and sensitivity with a visual detection limit as low as 11.35 ng mm^{-2} on the surface of the manila envelope.

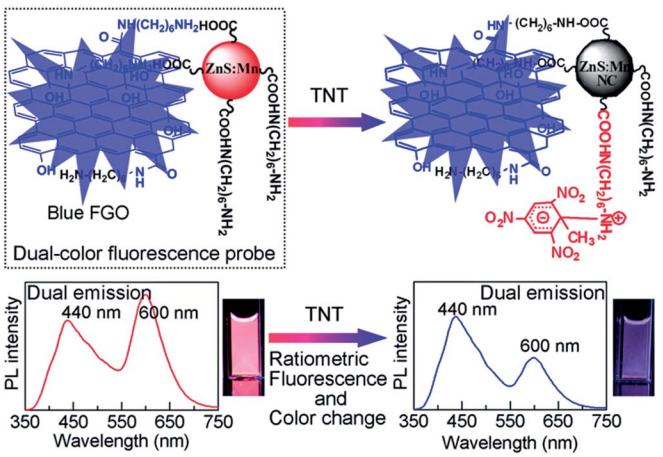

Scheme 1 Schematic illustration of the architecture of the nanohybrid probe and the working principle for the visual detection of TNT. The red-emissive 3-mercaptopropionic acid-capped nanocrystal is attached to the blue-emissive FGO surface. The hexamethylenediamine-bearing primary amino groups specifically reactive to TNT to form a Meisenheimer complex. The bottom panel shows the fluorescence changes of the probe upon exposure to a certain amount of TNT and the corresponding digital photos of the probe solution recorded under a UV lamp.

Experimental

Chemicals and materials

Zinc sulfate ($ZnSO_4 \cdot 7H_2O$), manganese acetate ($Mn(CH_3COO)_2 \cdot 4H_2O$), sodium sulfide ($Na_2S \cdot 9H_2O$), natural graphite flakes, *N*,*N*-dimethylformamide (DMF), dichloro sulfoxide, hexamethylenediamine (HMD), tetrahydrofuran (THF) and nitrobenzene (NB) were purchased from Sinopharm Chemical Reagent Co., Ltd. (Shanghai, China). 2,4,6-Trinitrotoluene (TNT) and 1,3,5-trinitro-1,3,5-triazinane (RDX) were supplied by the National Security Department of China, and were recrystallized with ethanol before use. 2,4-Dinitrotoluene (DNT) was purchased from Merck-Schuchardt (Hohenbrunn, Germany). 3-Mercaptopropionic acid (MPA), *N*-hydroxysuccinimide (NHS), and 1-(3-dimethylaminopropyl)-3-ethylcarbodiimide hydrochloride (EDC) were used as received from Sigma-Aldrich. Ultrapure water (18.2 MΩ cm) was obtained from a Millipore water purification system.

Synthesis of fluorescent graphene oxide (FGO)

FGO was synthesized using our previous method.[44] Typically, the dried graphene oxide (20 mg) was dispersed in 5 mL of DMF. Then 20 mL of dichloro sulfoxide was added into the solution and the mixture was refluxed at 80 °C for 48 h. After centrifugation at 10 000 rpm for 10 min, the supernatant was discarded and the remaining solid was washed with anhydrous tetrahydrofuran two times through centrifugation. The activated GO–acyl chloride (GO–COCl) and hexamethylenediamine (2 mL) were mixed and heated at 60 °C for 72 h. The resultant reaction solution was dispersed in ultrapure water (20 mL). A yellow supernatant was obtained after centrifugation at 8000 rpm for 10 min. The supernatant was then dried by rotary evaporation. The resultant hexamethylenediamine-modified FGO was re-dispersed in ultrapure water (20 mL). FGO showed bright blue fluorescence under UV illumination and the maximum fluorescence intensity was located at 440 nm with a 320 nm excitation.

Preparation and surface modification of manganese-doped ZnS nanocrystals (ZnS:Mn NCs)

14.775 g of $ZnSO_4 \cdot 7H_2O$ was dispersed in 80 mL of ultrapure water. An amount of 0.98 g manganese acetate was added into the above solution. The mixture was stirred under the protection of nitrogen for 0.5 h, and then 20 mL of aqueous solution containing 12.009 g of Na_2S was added into the reaction mixture. The resultant mixture was vigorously stirred for 3 h. The product ZnS:Mn NCs were obtained after centrifugation at 10 000 rpm for 10 min and then washed with ultrapure water several times through centrifugation. For the further surface modification, the product was re-dispersed in 120 mL of ultrapure water. 5 mL of the above solution was mixed with 0.36 mL of MPA (Zn–MPA = 1 : 2), and the mixture was stirred for 24 h under nitrogen atmosphere. The product was collected through centrifugation at 10 000 rpm for 10 min and washed with

ultrapure water several times to remove the residual MPA. Finally, the obtained nanocrystals were re-dispersed in 20 mL of ultrapure water for further use.

Synthesis of dual-color fluorescence nanohybrid probe

50 μL of HMD was mixed with 800 μL of mercaptoacetic acid-capped NCs and then 10 mL of a solution of EDC–NHS (1 mg mL^{-1}) was added. The mixture was stirred for 1 h at room temperature in the dark. Then, 1 mL of FGO was added, and the mixture was stirred for another 1 h. The resulting nanohybrids were obtained through centrifugation at 10 000 rpm for 10 min and then washed with ultrapure water to remove the excess FGO, free HMD and other chemicals. The nanohybrid probe was re-dispersed in 5 mL of ultrapure water (the concentration of probe solution is 15.2 mg mL^{-1}) for further use.

Measurements of fluorescence response to explosives

Typically, 10 μL of the stock probe solution was added to a spectrophotometer quartz cuvette. Subsequently, the solution was diluted to 2.0 mL by solvent (ethanol–acetonitrile, 4 : 1, v/v). The final concentration of probe solution for the fluorescence measurements was 76 μg mL^{-1}. The fluorescence spectra were recorded using a 320 nm excitation wavelength. All fluorescence measurements were performed at room temperature under ambient conditions. Meanwhile, the fluorescence responses of FGO and HMD-capped NCs were also measured by an identical procedure.

Visual detection of TNT residues on various surfaces

In order to prepare the test paper, 200 μL of probe solution was added into 10 mL of ultrapure water. The mixture was shaken for 5 min until the solution was evenly mixed. A piece of filter paper (40 mm × 35 mm; 40 mm × 25 mm) was immersed into the above mixture with ultrasonic agitation for 2 min. Then, the filter paper was removed from solution and kept still for 10 min in the dark. As the filter paper dries, it displays a strong red-colored fluorescence under a 312 nm UV lamp, indicating the successful preparation of the test paper. To visually detect TNT residues on surfaces, the test paper was contacted with the suspicious TNT-contaminated spots on these surfaces. In addition, 2.5 μL of different concentrations of TNT/acetonitrile solutions (0.5, 1, 2, 5 mM) were added dropwise on to the test paper and manila envelope, respectively. Spots of about 8 mm in diameter (contaminated area of about 50 mm^2) were formed after each deposition. The concentrations of TNT deposited on the surfaces (C: ng mm^{-2}) were estimated based on the TNT concentration in solution (C_0: mmol L^{-1}), solution volume (V: μL), and spot size (R: mm) formed after drying, according to the equation: $227C_0V/(\pi R^2)$. For each test, the test paper was contacted on all contaminated spots. The fluorescence color responses of the indicating paper were observed under a UV lamp (8 W, $\lambda_{max} = 312$ nm).

Characterizations

The fluorescence spectra were recorded using a Perkin-Elmer Luminescence Spectrometer LS-55 at room temperature. UV-visible absorbance spectra were obtained using a UNIC UV-4802 diode array spectrometer. The morphology of the nanohybrid was examined using a JEOL 2010 transmission electron microscope (TEM). All photographs were taken with a Canon 350D digital camera.

Results and discussion

In this work, we use FGO and ZnS:Mn NCs as luminescence units to construct the dual-color fluorescence nanohybrid probe. Compared with fluorescent semiconductor quantum dots (CdTe QDs, CdSe QDs, CdS QDs, and so forth), FGO and ZnS:Mn NCs are less toxic and greener for practical applications. The probe was obtained by simply mixing hexamethylenediamine (HMD)-modified graphene oxide[44] and MPA-capped NCs in water. The FGO was conjugated with the NCs among their surface capping molecules. Importantly, the amino groups of the HMD molecules act as the specific recognition sites for TNT. The fluorescence spectra of blue-emissive FGO, red-emissive MPA-capped NCs and the as-prepared dual-color fluorescence nanohybrid probe are shown in Fig. 1. FGO shows a fluorescence maximum at 440 nm and exhibits strong blue fluorescence under a UV lamp ($\lambda_{max} = 312$ nm). The NCs show two fluorescence maxima at 600 nm and 430 nm which are attributed to the characteristic $^4T_1 \rightarrow {}^6A_1$ transition of Mn^{2+} ions in the ZnS matrix and the defect-related emission of the ZnS, respectively.[47] Fortunately, the fluorescence intensity at 430 nm is much lower and does not interfere with the detection (Fig. 1b). After hybridization, the resultant nanohybrid probe displays well-resolved dual-emission bands under a single wavelength excitation at 320 nm (Fig. 1c). The nanohybrid probe exhibits a bright pink fluorescence color which is very different from the blue emission of FGO and the red emission of the NCs (inset images). These results indicate that the blue-emissive FGO is successfully conjugated with the red-emissive NCs and that both are photoluminescent under a single excitation. Investigations using infrared transmission spectroscopy have

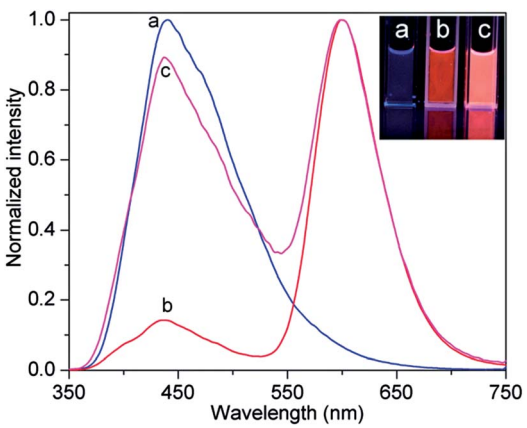

Fig. 1 Fluorescence emission spectra of (a) FGO, (b) MPA-capped NCs and (c) the dual-color fluorescence nanohybrid probe solution, and the corresponding fluorescence colors under a 312 nm UV lamp, respectively.

been carried out in order to prove the assumption of the formation of an amide bond between the primary amino group and the carboxyl group (Fig. S1 in ESI†). The IR absorption bands occur at 1550 cm^{-1} ($\nu_{as}COO^-$) and 1390 cm^{-1} (ν_sCOO^-) for the mercaptoacetic acid-capped nanocrystals.[52] Whereas the spectra of HMD-capped NCs and the nanohybrid probe show a broad band around 3200 cm^{-1} (νOH, H_2O and νNH_3^+), the bands at 3250 cm^{-1} (νNH(CONH)) and 1160 cm^{-1} (ν_{as}(C–N–C)) in the spectra indicate the existence of the amide bond. TEM images of the MPA-capped NCs and the nanohybrid probe are shown in Fig. S2 (see ESI†). As it can be seen, the NCs of 4–8 nm in diameter are well dispersed and then slightly aggregated before and after hybridization with FGO, respectively. The stability of the nanohybrid probe against photobleaching is systematically investigated in aqueous solution. After five consecutive illuminations at 320 nm (30 min for each time), the relative fluorescence intensity has no apparent change, implying its good photostability in aqueous solution (Fig. S3 in ESI†).

Scheme 1 illustrates the dual-color fluorescence nanohybrid probe structure and the working principle for the visual detection of TNT. The nanohybrid probe shows unique and well-resolved dual-emission bands under a single wavelength excitation (Scheme 1). As shown in our previous work,[36,37,45–47] the electron-withdrawing analyte, TNT, readily reacts with the electron-donating primary amino groups due to charge transfer from the amino groups to aromatic rings leading to the formation of Meisenheimer complexes, which often has a strong absorption in the visible range. The HMD molecules near the surface of the NCs thus have great reactivity to TNT to form a Meisenheimer complex, evidenced by UV-visible absorbance spectroscopy (Fig. 2). The anionic form of TNT can strongly absorb the visible light, leading to the color change of the solution (from colorless to pink). The TNT molecule is a Brønsted–Lowry acid and is deprotonated by interaction with an amino-group, leading to the formation of the anion–cation pair of TNT^- and RNH_3^+ in the solution. The charge of the complex is distributed throughout the TNT molecule and stabilized by resonance. Therefore, the amino groups at the surface of the NCs specifically recognize TNT molecules through the interaction. The resultant TNT anions bound to the surface of the nanohybrid probe quench the red fluorescence intensity of the NCs through electron transfer from the conductive band of ZnS to the lowest unoccupied molecular orbital of the TNT anions.[47] Meanwhile, the blue fluorescence intensity of FGO remains almost constant. The decrease of the red emission of the nanohybrid probe results in the color change of the total emission (from pink to blue), facilitating the visual detection of TNT.

The working principle of visual detection has been confirmed through monitoring the response of the dual-color fluorescence of the nanohybrid probe to TNT, as shown in Fig. 3. The nanohybrid probe exhibits two independent emission peaks, at 440 nm mainly from FGO, and 600 nm from the ZnS:Mn NCs. The intensity of the red emission is gradually decreased by the addition of TNT whereas the intensity of the blue emission remains almost unchanged. The changes in the fluorescent intensity ratio of the two emission wavelengths result in continuous color changes (a unique red–purple–blue fluorescence color response, as shown in the inset image of Fig. 3) which can be easily observed by the naked eye. Obviously, even a slight decrease of the red fluorescence leads to an obvious color change of the probe. Additionally, we have investigated the effect of pH values on the fluorescence process, and the results show that the ratio of the fluorescence quenching intensity was almost unaffected by pH values in the range of 6.06–8.05, as shown in Fig. S5.† These results demonstrate that the ratiometric measurement can avoid false-negatives generated by the pH change of the solution due to self-calibration of the two emission bands.

To demonstrate the more sensitive visual detection of the nanohybrid probe over that of the single-color fluorescence-based method, we have examined and compared the quenching effects of TNT on the fluorescence of FGO and HMD-capped

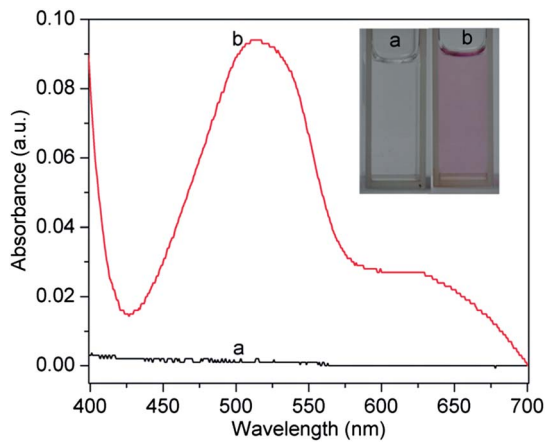

Fig. 2 Evolution of absorbance spectra of 2 mM of TNT solution (a) before and (b) after adding 10 μL of HMD. Inset image shows the corresponding color changes in natural light.

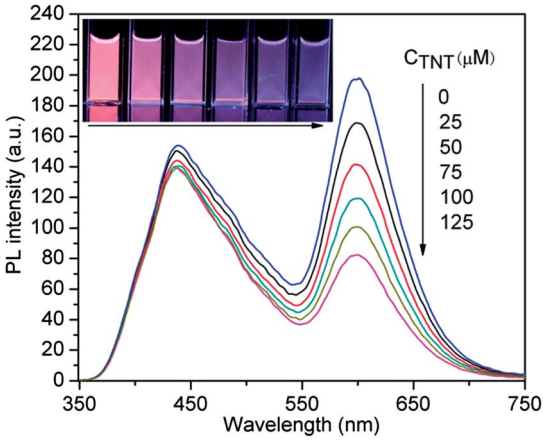

Fig. 3 The fluorescence spectra and the corresponding fluorescence color changes of the probe solution upon exposure to different concentrations of TNT. The concentrations of TNT from top to bottom are 0, 25, 50, 75, 100, 125 μM, respectively.

NCs (Fig. 4). It can be seen that TNT (125 μM) can only quench the blue fluorescence of FGO by 17%, which is ascribed to the strong molecular interaction between TNT and surplus hexamethylenediamine and/or the delocalized π-bond of graphene oxide. Although 17% of the fluorescence of FGO is quenched, the change of fluorescence color is negligible (inset images of Fig. 4A). Similarly, the fluorescence of HMD-capped NCs is greatly quenched by TNT, but the change of the fluorescence color is still hard to be distinguished by the naked eye (Fig. 4B inset images). In contrast, the same amount of TNT can generate a distinct fluorescence color change of the nanohybrid probe. Therefore, the comparison clearly demonstrates that the dual-color fluorescence method is more sensitive for the visual detection of TNT than the single-color fluorescence method. Actually, the detection of TNT with the mixture of FGO and HMD-capped NCs has been studied previously. Compared with the covalent conjugation probe, however, the simply mixed probe is less sensitive to TNT with the same concentration, as evidenced by the smaller changes in the intensity ratio (I_{600}/I_{440}) of the mixed probe (Fig. S6†).

The nanohybrid probe reacts with TNT in a dose–response manner, which can be utilized for quantitation of the analyte.[31] With the process of adding TNT, the intensity ratios of the two fluorescence peaks at 600 nm and 440 nm decrease gradually. As shown in Fig. 5, there is a highly linear calibration plot with a correlation coefficient $R^2 = 0.9998$ between the fluorescence emission intensity ratio (I_{600}/I_{440}) and the concentration of TNT at the micromolar level, allowing TNT to be monitored ratiometrically. Moreover, the nanohybrid probe also exhibits selectivity for TNT over other nitro-containing compounds including 2,4-dinitrotoluene (DNT), nitrobenzene (NB), and cyclotrimethylenetrinitramine (RDX). It can be seen in Fig. 5 that these nitro-compounds affect the fluorescence intensity ratio much less, even at higher concentrations, and hence no obvious fluorescence color changes result. In contrast, the fluorescence intensity ratio of the probe solution is decreased by about 60% by TNT with the concentration of 125 μM, resulting in remarkable fluorescence color changes under the UV lamp (see the inset image of Fig. 5). The results imply the high selectivity of the dual-color fluorescence nanohybrid probe for the visual identification of TNT over other nitro-containing explosives. These nitro-compounds show a quenching efficiency in the order: TNT ≫ DNT > NB > RDX, which suggests that the quenching efficiency is dependent upon the nitro-number, which is related to the electron-withdrawing ability of the analytes. As a non-aromatic compound, RDX has the lowest electron-withdrawing ability and does not have a specific acid–base interaction with the amino ligands at the surface of the NCs. Thus the probe can obviously distinguish TNT from these explosive compounds.

It is well documented that TNT can stick to and contaminate solid surfaces even with extremely cautious handling due to its strong adsorption and low vapor pressure.[48,49] So the instant, on-site, and visual detection of trace TNT residues on suspicious objects surfaces is crucial for security screening needs. For this purpose, we make test papers using the nanohybrid probe and common filter paper to detect trace TNT residues on various surfaces. We choose filter paper for it is inexpensive, available, easy to store and transport, and can be burned at the

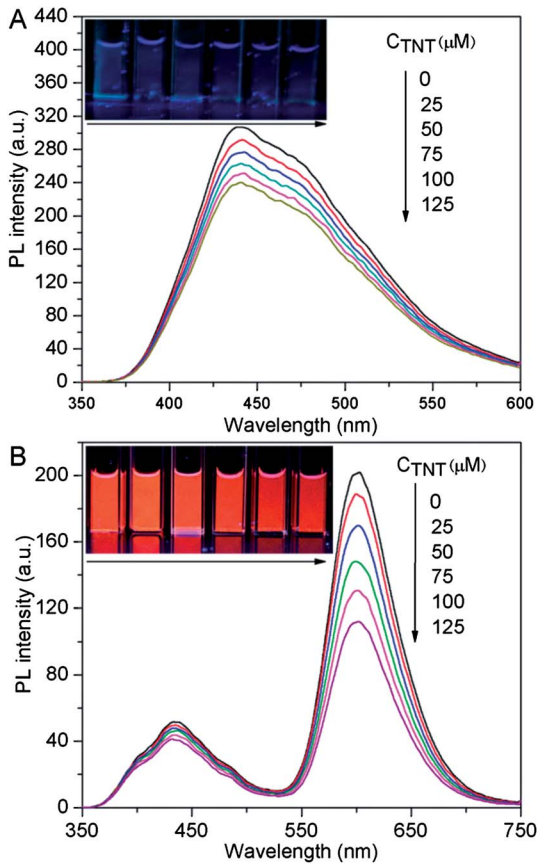

Fig. 4 The fluorescence spectra and the corresponding fluorescence color changes of (A) FGO and (B) HMD-capped NCs solution upon exposure to different concentrations of TNT. The concentrations of TNT from top to bottom are 0, 25, 50, 75, 100, 125 μM, respectively. The digital photos were taken under a UV lamp.

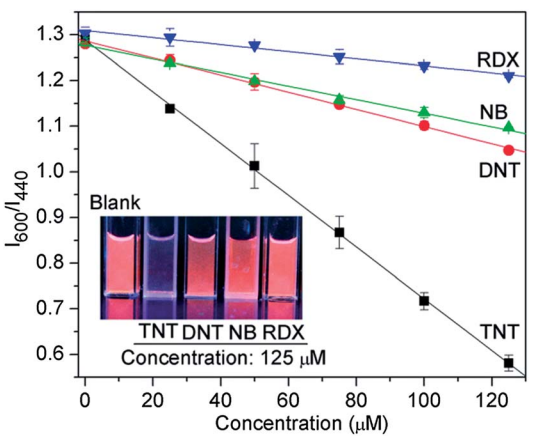

Fig. 5 Fluorescence emission intensity ratio (I_{600}/I_{400}) of the nanohybrid probe as a function of different concentrations of nitro-containing compounds, respectively. The inset image shows the corresponding color changes with the addition of 125 μM of different analytes.

conclusion of an assay for disposal.[50,51] The filter papers were immersed into the well-homogenized probe solution to adsorb the probe particles due to the hydrophilic and hydrogen-bonding interactions. The filter paper was then taken out and kept in the dark for 10 min before the test. The as-prepared test paper displays red fluorescence under a 312 nm UV lamp, as illustrated in Fig. 6A. After contacting with a rubber surface with the 'TNT' pattern made of TNT residues, an apparent pattern of 'TNT' of a different color was seen against the red background of the test paper. A fingerprint of a finger contaminated with TNT residues was also clearly visualized on the test paper (Fig. 6B). The contaminated fingerprint shows an obvious blue color whereas the negative control fingerprint without TNT shows no trace on the test paper. These results clearly demonstrate the utility of the test paper for visualizing the detection of trace residues of TNT. The visual detection limit, defined as the least amount of TNT on the surface capable of producing a different colored spot that can be noted by independent observers, is used for evaluating the analytical performance of the test paper. Trace TNT residues on the surface are simulated by depositing TNT/acetonitrile solution on a test paper, followed by drying in air. Different amounts of TNT were deposited on the surface and were estimated to be 56.75, 22.70, 11.35, 5.68 ng mm^{-2}, respectively. From Fig. 6C, it can be seen that each spot is distinct and displays the color change from dark blue (on the top-left corner) to shallow blue (on the bottom-right corner), and the visual detection limit of the test paper could be estimated to be 5.68 ng mm^{-2}. Moreover, trace TNT residues on a manila envelope surface are also clearly visualized using a similar procedure. TNT residues deposited on a manila envelope are captured by the formation of a Meisenheimer complex and lifted from the surface to the test paper. As shown in Fig. 6D, trace TNT residues are clearly revealed as different colored spots against the clear red background under the illumination of the UV lamp. Obviously, the patterns of the color spots are consistent with the corresponding areas of TNT residues. The visual detection limit for TNT on the manila envelope is measured to be 11.35 ng mm^{-2}, which is higher than that on the test paper. This could be due to the diffusion of TNT molecules into the depth of the envelope surface and they are hard to be adsorbed by the test paper. Furthermore, as nitroaromatic compounds are harmful to the environment, it is preferable for the test substrates to be destroyed by complete burning after sensing. So such test papers are considerably greener and more eco-friendly to avoid environmental contamination (Fig. 6E).

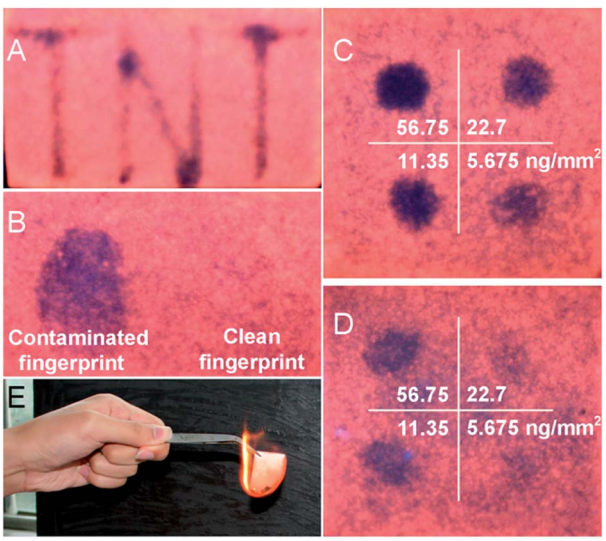

Fig. 6 The color images of test papers for the visual detection of trace TNT residues on various surfaces. (A) TNT print on rubber surface; (B) fingerprints with and without TNT contaminant pressed onto the test paper; test papers capture TNT residues deposited on (C) a test paper surface, and (D) a manila envelope surface with different amounts of 56.75, 22.7, 11.35, and 5.68 ng mm^{-2}; (E) a test paper is burned after sensing to avoid TNT pollution in the environment.

Conclusions

In summary, we have demonstrated a novel method and utility for the visual detection of TNT residues in solution and on various surfaces. The method based on the dual-color fluorescence nanohybrid probe comprising the blue-emissive FGO and red-emissive NCs could be utilized for the quantitative measurement of TNT based on fluorescence ratiometry and color changes. Compared with a single-color fluorescence probe, this method exhibits significantly enhanced visual detection sensitivity and reliability. Moreover, the nanohybrid probe has been successfully made into test papers for detecting trace TNT residues on various surfaces including rubber, a person's fingers and manila envelopes, which validate the efficiency of instant, on-site, and visual identification of TNT and could be extended to the visual detection of a wide range of organic and inorganic molecules.

Acknowledgements

This work was supported by the National Basic Research Program of China (2011CB933700), the Natural Science Foundation of China (no. 21205120, 21173229) and the Innovation Project of Chinese Academy of Sciences (KJCX2-YW-H29).

References

1 J. Yinon, *Anal. Chem.*, 2003, **75**, 99A–105A.
2 J. I. Steinfeld and J. Wormhoudt, *Annu. Rev. Phys. Chem.*, 1998, **49**, 203–232.
3 D. S. Moore, *Rev. Sci. Instrum.*, 2004, **75**, 2499–2512.
4 S. Singh, *J. Hazard. Mater.*, 2007, **144**, 15–28.
5 R. G. Smith, N. D'Souza and S. Nicklin, *Analyst*, 2008, **133**, 571–584.
6 J. Yinon, *TrAC, Trends Anal. Chem.*, 2002, **21**, 292–301.
7 Y. Jiang, H. Zhao, N. N. Zhu, Y. Q. Lin, P. Yu and L. Q. Mao, *Angew. Chem., Int. Ed.*, 2008, **47**, 8601–8604.
8 Y. Zhang, X. X. Ma, S. C. Zhang, C. D. Yang, Z. Ouyang and X. R. Zhang, *Analyst*, 2009, **134**, 176–181.
9 J. Yinon, *J. Chromatogr., A*, 1996, **742**, 205–209.

10 N. L. Sanders, S. Kothari, G. M. Huang, G. Salazar and R. G. Cooks, *Anal. Chem.*, 2010, **82**, 5313–5316.
11 N. Talaty, C. C. Mulligan, D. R. Justes, A. U. Jackson, R. J. Noll and R. G. Cooks, *Analyst*, 2008, **133**, 1532–1540.
12 M. Tam and H. H. Hill, *Anal. Chem.*, 2004, **76**, 2741–2747.
13 M. Najarro, M. E. D. Morris, M. E. Staymates, R. Fletcher and G. Gillen, *Analyst*, 2012, **137**, 2614–2622.
14 K. Qian, H. L. Liu, L. B. Yang and J. H. Liu, *Analyst*, 2012, **137**, 4644–4646.
15 E. M. A. Ali, H. G. M. Edwards and I. J. Scowen, *J. Raman Spectrosc.*, 2009, **40**, 2009–2014.
16 S. S. R. Dasary, A. K. Singh, D. Senapati, H. T. Yu and P. C. Ray, *J. Am. Chem. Soc.*, 2009, **131**, 13806–13812.
17 M. R. Leahy-Hoppa, M. J. Fitch, X. Zheng, L. M. Hayden and R. Osiander, *Chem. Phys. Lett.*, 2007, **434**, 227–230.
18 W. H. Fan, A. Burnett, P. C. Upadhya, J. Cunningham, E. H. Linfield and A. G. Davies, *Appl. Spectrosc.*, 2007, **61**, 638–643.
19 B. Sun, M. Q. Li, F. Zhang, Y. Zhong, N. S. Kang, W. Lu and J. H. Liu, *Microchem. J.*, 2010, **95**, 293–297.
20 L. L. Stevens, N. Velisavljevic, D. E. Hooks and D. M. Dattelbaum, *Propellants, Explos., Pyrotech.*, 2008, **33**, 286–295.
21 S. J. Toal and W. C. Trogler, *J. Mater. Chem.*, 2006, **16**, 2871–2883.
22 M. S. Meaney and V. L. McGuffin, *Anal. Bioanal. Chem.*, 2008, **391**, 2557–2576.
23 M. E. Germain and M. J. Knapp, *Chem. Soc. Rev.*, 2009, **38**, 2543–2555.
24 L. Senesac and T. G. Thundat, *Mater. Today*, 2008, **11**, 28–36.
25 S. Zahn and T. M. Swager, *Angew. Chem., Int. Ed.*, 2002, **41**, 4225–4230.
26 J. S. Yang and T. M. Swager, *J. Am. Chem. Soc.*, 1998, **120**, 5321–5322.
27 J. S. Yang and T. M. Swager, *J. Am. Chem. Soc.*, 1998, **120**, 11864–11873.
28 A. Rose, Z. G. Zhu, C. F. Madigan, T. M. Swager and V. Bulovic, *Nature*, 2005, **434**, 876–879.
29 Y. Salinas, R. Martinez-Manez, M. D. Marcos, F. Sancenon, A. M. Costero, M. Parra and S. Gil, *Chem. Soc. Rev.*, 2012, **41**, 1261–1296.
30 E. R. Goldman, I. L. Medintz, J. L. Whitley, A. Hayhurst, A. R. Clapp, H. T. Uyeda, J. R. Deschamps, M. E. Lassman and H. Mattoussi, *J. Am. Chem. Soc.*, 2005, **127**, 6744–6751.
31 K. Zhang, H. Zhou, Q. Mei, S. Wang, G. Guan, R. Liu, J. Zhang and Z. Zhang, *J. Am. Chem. Soc.*, 2011, **133**, 8424–8427.
32 Y. S. Xia, L. Song and C. Q. Zhu, *Anal. Chem.*, 2011, **83**, 1401–1407.
33 W. S. Zou, D. Sheng, X. Ge, J. Q. Qiao and H. Z. Lian, *Anal. Chem.*, 2011, **83**, 30–37.
34 A. Mathew, P. R. Sajanlal and T. Pradeep, *Angew. Chem., Int. Ed.*, 2012, **51**, 9596–9600.
35 Y. X. Ma, H. Li, S. Peng and L. Y. Wang, *Anal. Chem.*, 2012, **84**, 8415–8421.
36 J. L. Geng, P. Liu, B. H. Liu, G. J. Guan, Z. P. Zhang and M. Y. Han, *Chem. – Eur. J.*, 2010, **16**, 3720–3727.
37 D. M. Gao, Z. Y. Wang, B. H. Liu, L. Ni, M. H. Wu and Z. P. Zhang, *Anal. Chem.*, 2008, **80**, 8545–8553.
38 P. T. Snee, R. C. Somers, G. Nair, J. P. Zimmer, M. G. Bawendi and D. G. Nocera, *J. Am. Chem. Soc.*, 2006, **128**, 13320–13321.
39 V. V. Shynkar, A. S. Klymchenko, C. Kunzelmann, G. Duportail, C. D. Muller, A. P. Demchenko, J. M. Freyssinet and Y. Mely, *J. Am. Chem. Soc.*, 2007, **129**, 2187–2193.
40 M. Wang, Q. S. Mei, K. Zhang and Z. P. Zhang, *Analyst*, 2012, **137**, 1618–1623.
41 Y. Kubo, M. Yamamoto, M. Ikeda, M. Takeuchi, S. Shinkai, S. Yamaguchi and K. Tamao, *Angew. Chem., Int. Ed.*, 2003, **42**, 2036–2040.
42 P. Wu, T. Zhao, S. L. Wang and X. D. Hou, *Nanoscale*, 2014, **6**, 43–64.
43 S. Sen, S. Sarkar, B. Chattopadhyay, A. Moirangthem, A. Basu, K. Dhara and P. Chattopadhyay, *Analyst*, 2012, **137**, 3335–3342.
44 Q. S. Mei, K. Zhang, G. J. Guan, B. H. Liu, S. H. Wang and Z. P. Zhang, *Chem. Commun.*, 2010, **46**, 7319–7321.
45 D. M. Gao, Z. P. Zhang, M. H. Wu, C. G. Xie, G. J. Guan and D. P. Wang, *J. Am. Chem. Soc.*, 2007, **129**, 7859–7866.
46 Q. L. Fang, J. L. Geng, B. H. Liu, D. M. Gao, F. Li, Z. Y. Wang, G. J. Guan and Z. P. Zhang, *Chem. – Eur. J.*, 2009, **15**, 11507–11514.
47 R. Y. Tu, B. H. Liu, Z. Y. Wang, D. M. Gao, F. Wang, Q. L. Fang and Z. P. Zhang, *Anal. Chem.*, 2008, **80**, 3458–3465.
48 A. Macek, *Chem. Rev.*, 1962, **62**, 41–63.
49 M. N. Chaffee-Cipich, B. D. Sturtevant and S. P. Beaudoin, *Anal. Chem.*, 2013, **85**, 5358–5366.
50 H. Sohn, R. M. Calhoun, M. J. Sailor and W. C. Trogler, *Angew. Chem., Int. Ed.*, 2001, **40**, 2104–2105.
51 S. J. Toal, J. C. Sanchez, R. E. Dugan and W. C. Trogler, *J. Forensic Sci.*, 2007, **52**, 79–83.
52 K. Hoppe, E. Geidel, H. Weller and A. Eychmuller, *Phys. Chem. Chem. Phys.*, 2002, **4**, 1704–1706.